Available online at www.sciencedirect.com
ScienceDirect
Materials Research Bulletin 43 (2008) 2119–2129
Materials Research Bulletin
www.elsevier.com/locate/matresbu

# Phthalic acid assisted nano-sized spinel $LiMn_2O_4$ and $LiCr_xMn_{2-x}O_4$ ($x = 0.00$–$0.40$) via sol–gel synthesis and its electrochemical behaviour for use in Li-ion-batteries

R. Thirunakaran [a,b,*], A. Sivashanmugam [a], S. Gopukumar [a], Charles W. Dunnill [b], Duncan H. Gregory [b]

[a] *Central Electrochemical Research Institute, Karaikudi 630006, Tamil Nadu, India*
[b] *University of Glasgow, Chemistry Department, Glasgow G12 8QQ, United Kingdom*

Received 2 July 2007; received in revised form 17 September 2007; accepted 17 September 2007
Available online 29 September 2007

**Abstract**

Nano-sized particles of spinel $LiMn_2O_4$ and $LiCr_xMn_{2-x}O_4$ ($x$ = Cr; 0.00–0.40) have been synthesized using phthalic acid as chelating agent for the first time by sol–gel method. When compared to solid-state synthesis method, the sol–gel route reduces heating time of synthesize and to obtain particles of uniform surface morphology. The synthesized samples were characterized through thermo-gravimetric analysis (TGA), X-ray diffraction (XRD), scanning electron microscopy (SEM) and transmission electron microscopy (TEM). SEM images of the parent compounds show nanospherical grains of $LiMn_2O_4$ when compared to chromium-doped ones. XRD patterns of $LiMn_2O_4$ ascertain amorphous nature and for high calcined $LiCr_xMn_{2-x}O_4$ single phase highly crystalline patterns were obtained. TEM images of the parent and chromium-doped spinel particles depict individual grain morphology with well-separated grain boundaries. $LiCr_{0.10}Mn_{1.90}O_4$ excels in discharge and cycling behaviour and offer higher columbic efficiency, when compared to un-doped $LiMn_2O_4$. Cyclic voltammograms of $LiMn_2O_4$ and $LiCr_xMn_{2-x}O_4$ exhibit oxidation and reduction peaks corresponding to $Mn^{3+}/Mn^{4+}$ and $Cr^{3+}/Cr^{4+}$.


*Keywords:* B. Intercalation reactions; B. Sol–gel chemistry; C. X-ray diffraction; D. Electrochemical properties; D. Energy storage

## 1. Introduction

Pure spinel $LiMn_2O_4$ is one of the most promising candidates for rechargeable lithium batteries due its low cost, non-toxic and ease of preparation when compared to other layered oxides such as $LiCoO_2$, and $LiNiO_2$ [1–3]. The capacity of pure spinel $LiMn_2O_4$ upon repeated cycling diminishes at elevated temperature which has been reported by several authors [4,5]. The capacity fade is caused due to the several factors such as Jahn–Teller distortion, two-phase unstable reaction [6], and slow dissolution of manganese into the electrolyte [7], lattice instability [8], and particle size distribution [9]. Of late, several metal cations such as Co, Zn, Cu, Fe, Ni, Cr, Ti, and Al have been doped in $LiMn_2O_4$ [10,11] spinel to suppress the Jahn–Teller distortion for obtaining high capacity over repeated cycling. Ohuzuku et al. [9] and Lee et al. [12] reported earlier that partial doping of divalent and trivalent cations are more effective in

* Corresponding author. Fax: +91 4565 227779.
*E-mail address:* rthirunakaran@yahoo.com (R. Thirunakaran).

0025-5408/$ – see front matter © 2007 Elsevier Ltd. All rights reserved.
doi:10.1016/j.materresbull.2007.09.021

suppressing the capacity fade up on cycling. Further, the capacity fade of $LiMn_2O_4$ is often observed much in the 3 V region which can be completely suppressed by doping selenium with $LiMn_2O_4$ [13]. In recent years, several low temperature preparation methods viz., sol–gel method [14,15], precipitation [16], pechini process [17], and hydrothermal method [18] have been used for synthesizing $LiMn_2O_4$ with desired physical and electrochemical properties to use as cathode material for rechargeable lithium-ion-batteries.

In this work, an attempt has been made for the first time, to use phthalic acid as chelating agent to stabilize $LiMn_2O_4$ spinel structure by green chemistry route with trivalent cation substitution ($LiCr_xMn_{2-x}O_4$: $x$ = Cr: 0.00–0.40). Undoubtedly, sol–gel method offers many advantages such as sub-micron sized particles, shorter heating time, regular morphology, good agglomeration behaviour, better homogeneity, less particle size, high surface area and no-by product [10].

## 2. Experimental

Spinel $LiMn_2O_4$ and $LiCr_xMn_{2-x}O_4$: ($x$ = Cr: 0.00–0.40) powders have been synthesized by sol–gel method using phthalic acid as chelating agent. Fig. 1 shows the flow chart of the synthesis procedure. Stoichiometric amounts of lithium acetate, manganese acetate and chromium acetate were mixed thoroughly and dissolved in de-ionized water. This solution was stirred constantly with mild heating (60 °C) till it reaches complete homogeneity. Fifty milliliters of 1 M phthalic acid was added to the homogenous solution and stirred continuously during which the pH was measured to be in slightly acidic range of 5–6 which might enhance the chelation of metal ligands and thereby a foamy gel was obtained. Samples were taken for TGA to understand the thermal behaviour of the compound. Simultaneously, the gel was dried overnight in an oven at 110 °C for removing moisture and to obtain a dried mass. Finally, the powder was calcined at different temperatures viz., 250, 450, 650 and 850 °C for 4 h. The calcined samples were subjected to various spectral studies for physical characterization and finally for electrochemical studies. X-ray Diffractometer

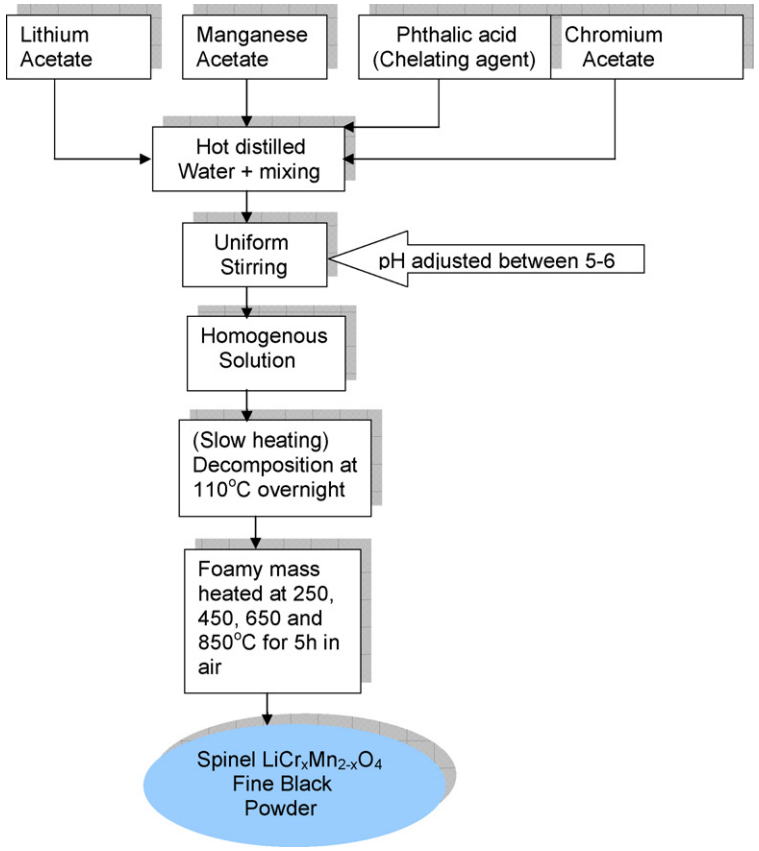


Fig. 1. Flow chart for synthesis of $LiCr_xMn_{2-x}O_4$ by a sol–gel method using phthalic acid as a chelating agent.

D5000, SIEMENS, scanning electron microscope JEOL, SEM 500, Japan, transmission electron microscope JEM-1200EX, Japan and thermo-gravimetric analyser SDT Q600 were used for characterization.

### 2.1. Coin cell preparation

Coin cells of 2016 configuration were assembled using lithium metal as anode, Celgard 2400 as separator and 1 M solution of $LiPF_6$ dissolved in 50:50 (v/v) mixture of ethylene carbonate (EC) and diethylene carbonate (DEC) as electrolyte. The cathode slurry consists of active material, carbon black and poly(vinylidene fluride) PVdF binder in *N*-methyl-2-pyrrolidone (NMP) in the ratio 80:10:10. The slurry was coated over aluminium foil and dried in an oven at 110 °C for 2 h. The coated foil was pressed at 10 tonnes kg $cm^{-2}$ for 2 min and the electrodes of 18 mm diameter was punched out. Coin cells were assembled in an argon filled glove box (MBraun, Germany) and used for electrochemical studies. These cells were cycled galvanostatically in a battery cycling unit at C/10 rate. Some cells were subjected to cyclic voltammetry studies wherein lithium foil act as counter and reference electrode.

## 3. Results and discussion

### 3.1. Thermal studies

Fig. 2 shows thermo-gravimetric analysis (TGA) of spinel $LiMn_2O_4$ precursor. The TG curve depicts several weight loss regions. The weight loss region (less than 1%) up to 200 °C can be attributed to the removal of moisture. The following multiple weight loss regions observed between 200 and 700 °C corresponding to weight loss of 55% is associated with the decomposition reaction of the acetate precursors and chelating agent. This can be supplemented from the XRD results that the peak signatures of $LiMn_2O_4$ are indistinct for the as synthesized and the calcined ones at 250 °C. Characteristic peaks corresponding to $LiMn_2O_4$ spinel starts appearing after 450 °C. Further, the presence of impurity peaks in the XRD patterns corresponding to the low calcined samples at 450 and 650 °C substantiate the progression of the reaction which is reflected in the TGA curve by way of the several weight loss zones until 700 °C. Gravimetrically stable region above 750 °C declares the completion of the reaction as can be ratified by the fingerprint peaks obtained for $LiMn_2O_4$ spinel calcined at 850 °C.

Fig. 3 shows thermo-gravimetric analysis of $LiCr_xMn_{2-x}O_4$ precursor with different Cr-doping levels viz., (a) Cr-0.10; (b) Cr-0.20; (c) Cr-0.30; (d) Cr-0.40. The TGA pattern of the chromium-doped spinel follows a similar behaviour to that of parent $LiMn_2O_4$ spinel. The first weight loss region (4%) extending up to 300 °C is accounted for the removal of moisture. Further stepwise weight loss zones amounting to 58% observed beyond 400 °C are corresponding to the decomposition of acetate precursors. Increase in chromium doping shows a marginal raise in weight loss. Flatness in TGA curve above 800 °C vindicates the completion of thermal events.

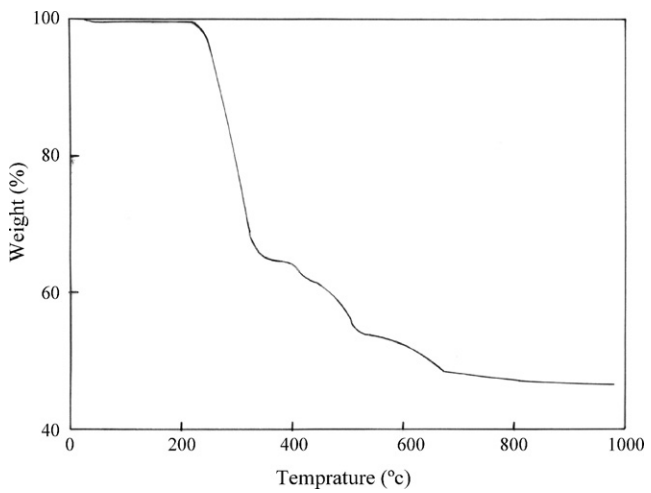


Fig. 2. Thermo-gravimetric analysis of spinel $LiMn_2O_4$ precursor.

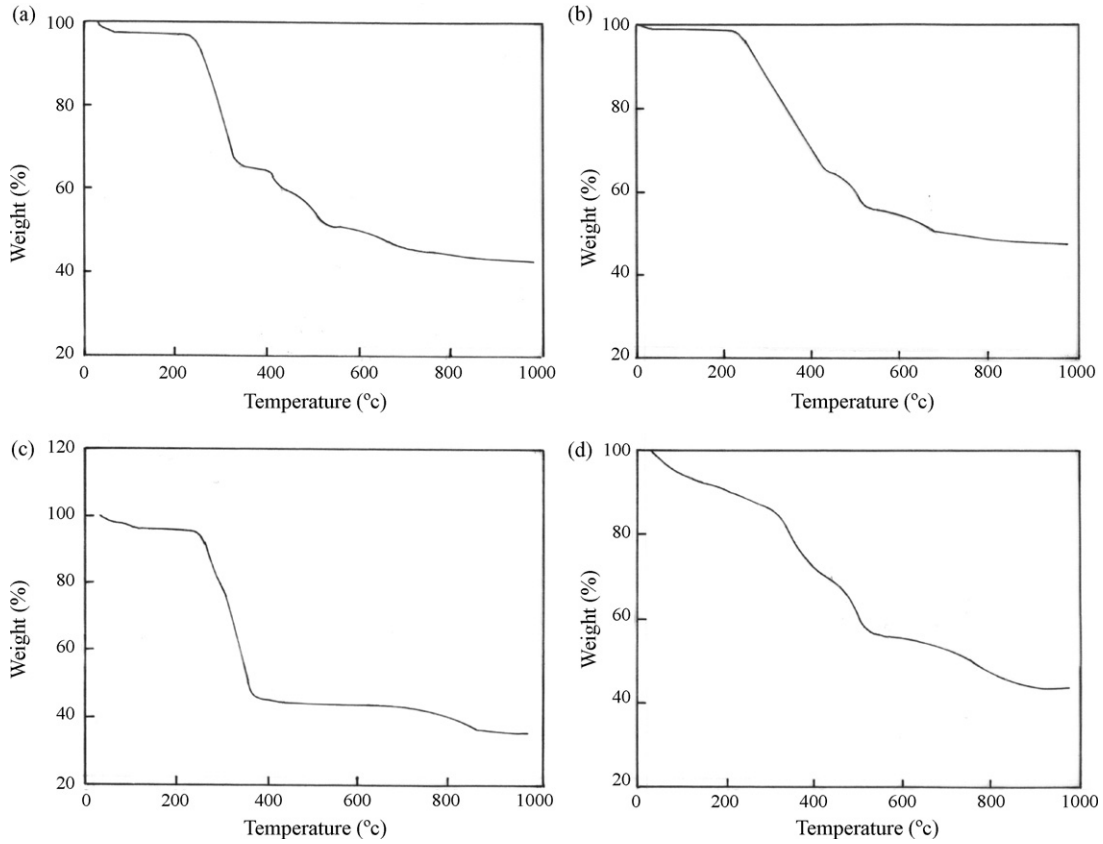


Fig. 3. Thermo-gravimetric analysis of $LiCr_xMn_{2-x}O_4$ precursor with different Cr-doping levels viz., (a) Cr-0.10; (b) Cr-0.20; (c) Cr-0.30; (d) Cr-0.40.

### 3.2. X-ray diffraction

Fig. 4 shows the XRD patterns of as synthesized and calcined $LiMn_2O_4$ samples at different temperatures. The XRD patterns of as synthesized and calcined $LiMn_2O_4$ at 250 °C samples show that the materials are highly amorphous in nature. Few additional peaks corresponding to $\alpha$-$Mn_2O_3$ and $LiMn_2O_3$ were observed in the XRD patterns of the samples calcined at 250 and 450 °C. Further, with increase in calcination temperature to 650 and 850 °C ensured better phase purity and crystallinity of the compound. The XRD pattern of the sample heated at 850 °C substantiates the formation of highly crystalline product. The peak signatures were indexed to the indices (1 1 1), (2 2 0), (3 1 1), (2 2 2), (4 0 0), (3 3 1), (5 5 1), (4 4 0) and (3 5 1), respectively which are in good agreement with that of standards reported by several researchers [19–21].

Fig. 5 shows the XRD patterns of $LiMn_2O_4$ and $LiCr_xMn_{2-x}O_4$ with different Cr-doping levels viz., 0.10, 0.20, 0.30 and 0.40 synthesized through sol–gel method calcined at 850 °C. All the XRD peaks corresponding to (1 1 1), (2 2 0), (3 1 1), (2 2 2), (4 0 0), (3 3 1), (5 5 1), (4 4 0) and (3 5 1) planes observed for $LiMn_2O_4$ and $LiCr_xMn_{2-x}O_4$ [22–24] sampled hold striking similarity to JCPDS card No. 35-782 thereby confirming the formation of single phase spinel compound. However, for low calcined (250 and 450 °C) samples, additional peaks observed in (2 2 2), (2 2 0), (3 3 1) and (3 5 1) planes may be due to the presence of $\alpha$-$Mn_2O_3$ and $LiMn_2O_3$. Hence it is evident that phthalic acid as a chelating agent forms metal ligands chain easily between Mn–O and COO group particles resulting in the formation of $LiCr_xMn_{2-x}O_4$ spinel product.

### 3.3. Scanning electron microscopy

Fig. 6 shows the SEM images of spinel $LiMn_2O_4$ particles calcined at different temperatures viz., 250, 450, 650 and 850 °C. The image for $LiMn_2O_4$ powder calcined at 250 °C shows that the particles are below 50 nm in size.

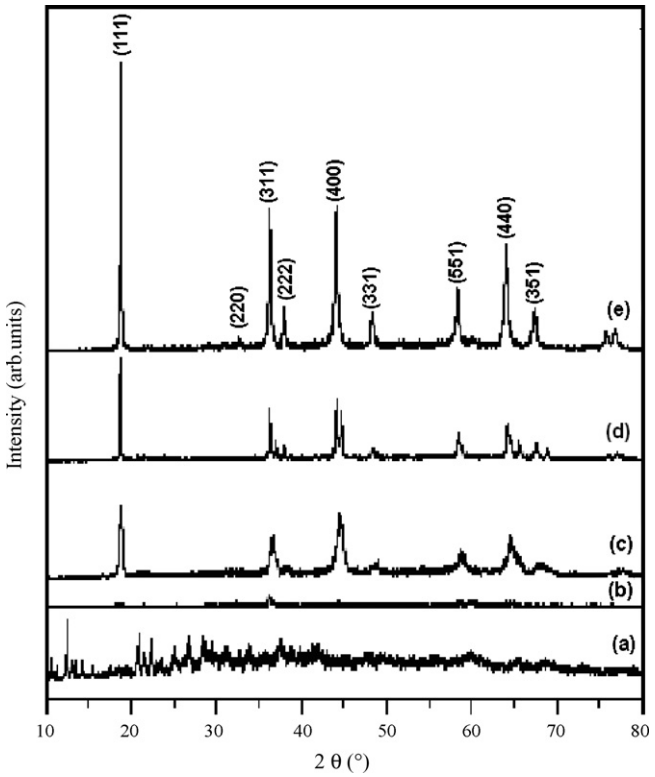


Fig. 4. XRD patterns of $LiMn_2O_4$ samples calcined at different temperatures: (a) as synthesized; (b) 250 °C; (c) 450 °C; (d) 650 °C; (e) 850 °C.

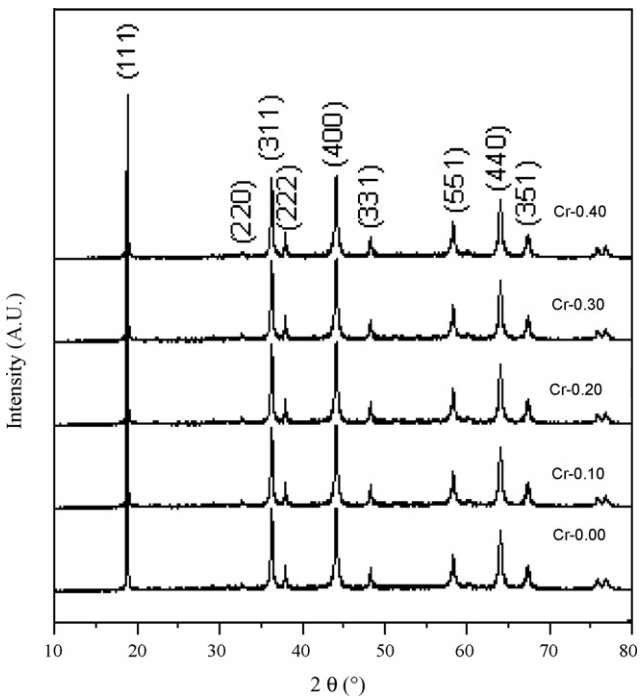


Fig. 5. XRD patterns of $LiMn_2O_4$ and $LiCr_xMn_{2-x}O_4$ ($x = 0.10$, 0.20, 0.30 and 0.40) calcined at 850 °C.

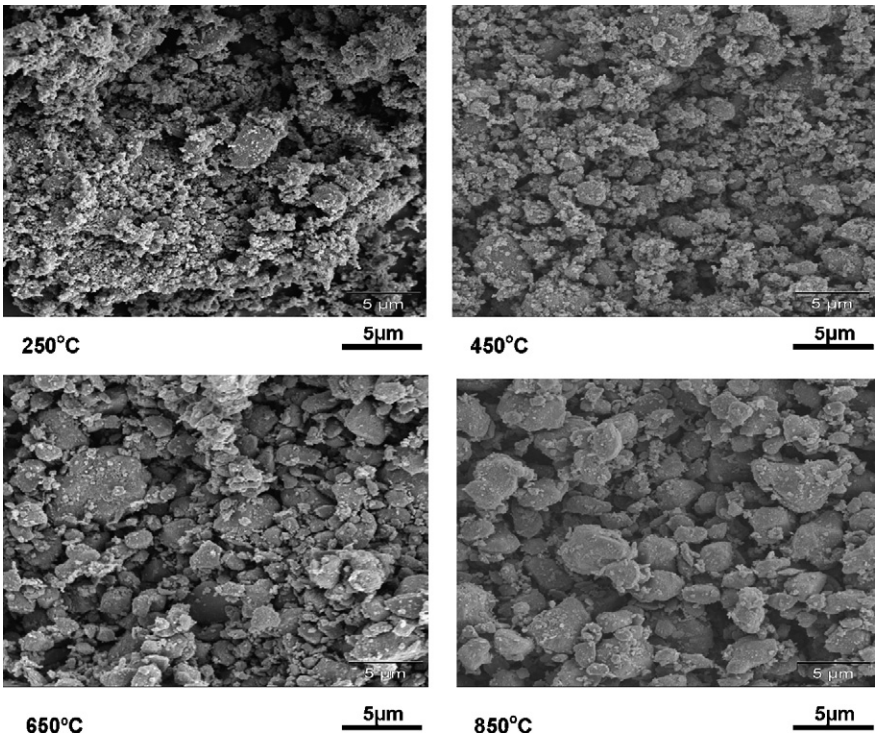


Fig. 6. SEM images of $LiMn_2O_4$ powder calcined at different temperatures (250, 450, 650 and 850 °C).

It is evident that the particles grow in size with increase in calcination temperatures (650 and 850 °C). Fig. 7 shows the SEM images of $LiMn_2O_4$ particles calcined at 850 °C with different Cr-doping. It is interesting to note that high Cr-doping (0.30 and 0.40 Cr) resulting to the formation of larger grains (around 1 μm) while at lower chromium concentrations ($x = 0.10$ and 0.20) the particles remain as fines of average grain size below 100 nm.

### 3.4. Transmission electron microscopy

Fig. 8 shows TEM images of spinel $LiMn_2O_4$ particles calcined at different temperatures viz., 250, 450, 650 and 850 °C. It is obvious that the average particle size of the compound calcined at 250 and 450 °C is found to be around 100 nm. A portion of smaller particles are also seen. Further, it can be seen that particles depict individual grain morphology and well-separated grain boundaries and the grain size is found to be grown with increase in calcination temperature (650 and 850 °C). Fig. 9 shows TEM images $LiCr_xMn_{2-x}O_4$ particles with different Cr-dopant level calcined at 850 °C. Samples with high chromium (0.40) also present as well-separated grain boundary with individual grain morphology [25].

### 3.5. Charge–discharge studies

First cycle charge–discharge curves of sol–gel derived $LiMn_2O_4$ and $LiCr_xMn_{2-x}O_4$ powders with different Cr stoichiometry viz., $x = 0.10$, 0.20, 0.30 and 0.40 calcined at 850 °C and their cycling performance curves over 10 cycles and their corresponding columbic efficiencies (CE) are presented in Figs. 10 and 11. All samples show two distinct discharge plateaus. These are attributed to orderly intercalation of lithium ions in the tetrahedral (8a) sites at 4.1 V and disorderly intercalating lithium ions at 3.9 V [26–29]. Un-doped spinel $LiMn_2O_4$ calcined at 850 °C delivered discharge capacity around 135 mAh $g^{-1}$ against the charge capacity of 145 mAh $g^{-1}$ corresponding to 95% columbic efficiency during the first cycle. These cells show a fading cycling feature. In the 10th cycle these cells deliver 94 mAh $g^{-1}$ amounting to capacity fade of 4.1 mAh/(g cycle).

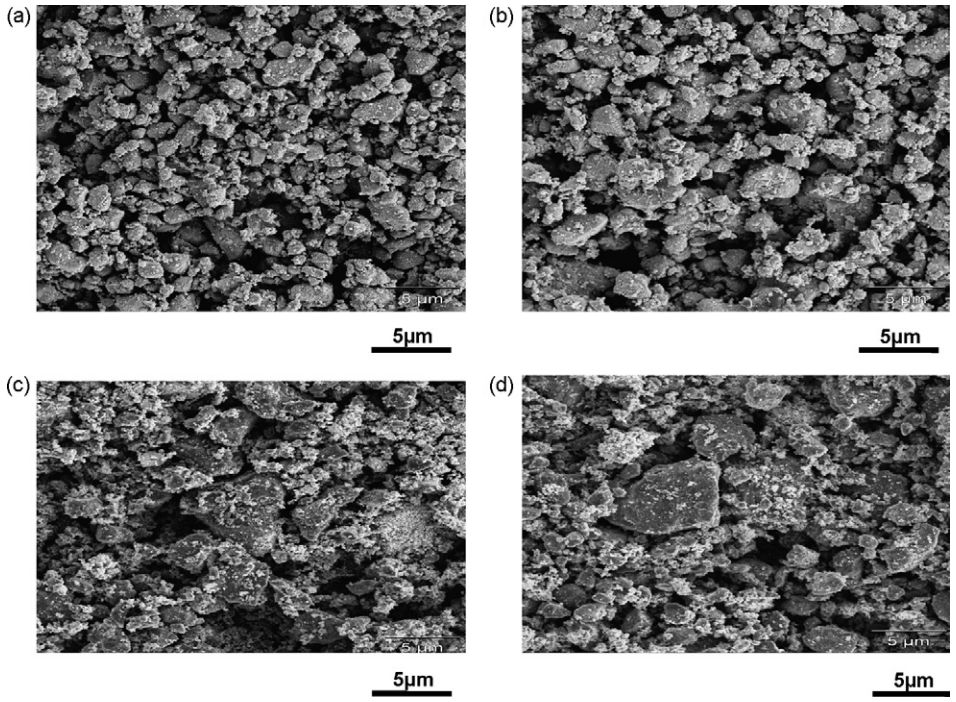


Fig. 7. SEM images of $LiCr_xMn_{2-x}O_4$ powders calcined at 850 °C with different Cr-doping levels viz., (a) Cr-0.10; (b) Cr-0.20; (c) Cr-0.30; (d) Cr-0.40.

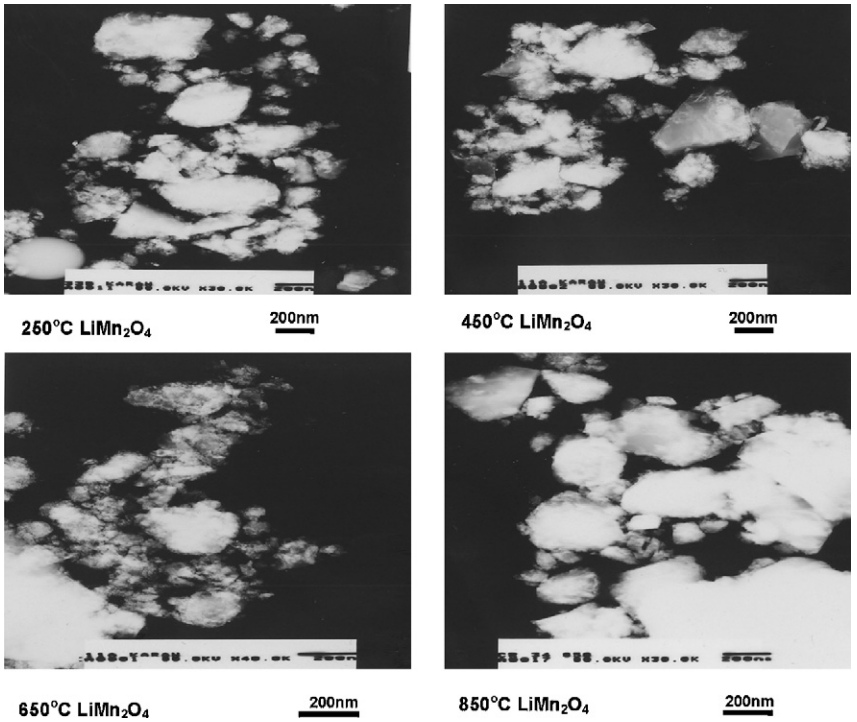


Fig. 8. TEM images of $LiMn_2O_4$ particles calcined at different temperatures (250, 450, 650 and 850 °C).

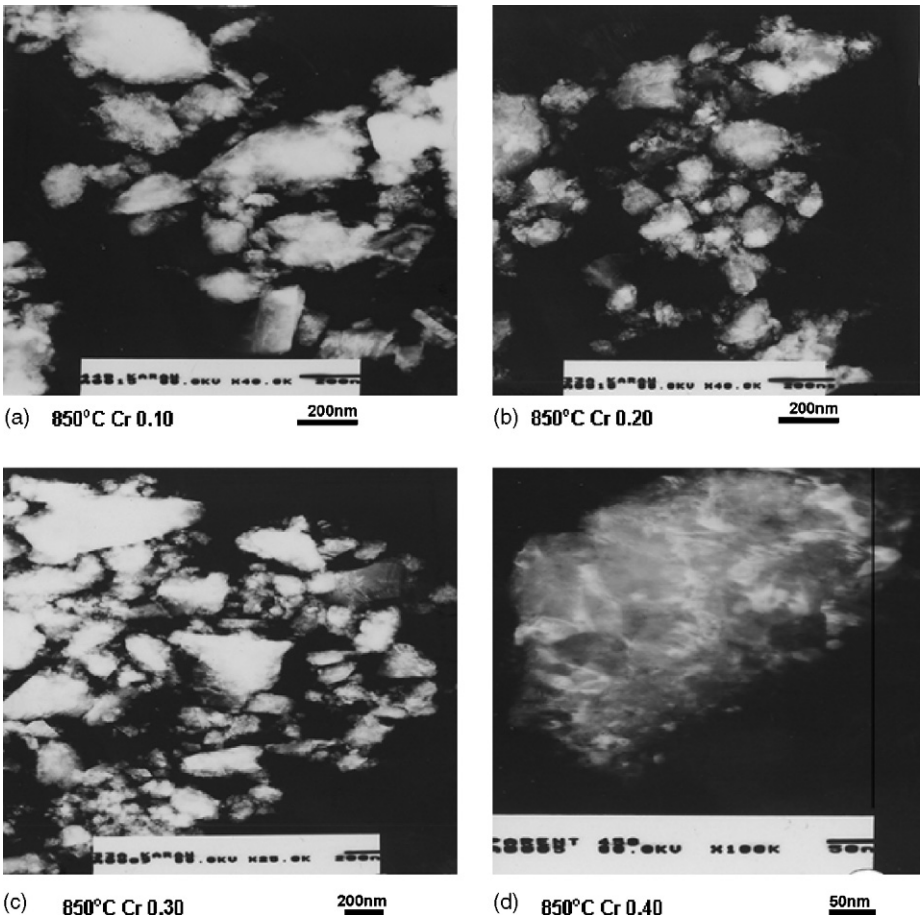


Fig. 9. TEM images of $LiCr_xMn_{2-x}O_4$ particles calcined at 850 °C with different Cr-doping levels viz., (a) Cr-0.10; (b) Cr-0.20; (c) Cr-0.30; (d) Cr-0.40.

In the case of Cr-doped spinels, it is interesting to note that, a slight increase in charge–discharge performance is observed when compared to un-doped $LiMn_2O_4$ at lower doping level of chromium (up to 0.2). Further, 0.10 Cr stoichiometry exhibits discharge capacity of 138 mAh $g^{-1}$ where as the same is 126 mAh $g^{-1}$ for 0.4 Cr. These results are superior to that of Zhang et al. [30] wherein $LiCr_{0.1}Mn_{1.9}O_4$ electrodes Exhibit 118 mAh $g^{-1}$ as first discharge

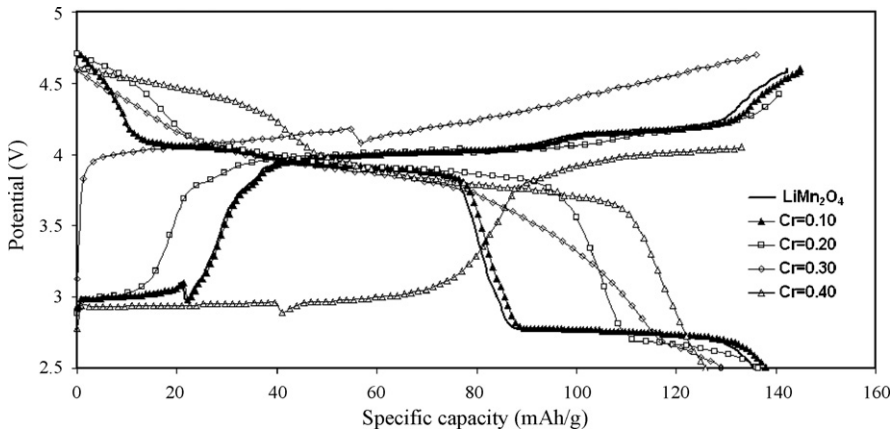


Fig. 10. Typical charge–discharge profiles of $LiMn_2O_4$ and $LiCr_xMn_{2-x}O_4$ samples with different Cr-doping levels viz., 0.10, 0.20, 0.30 and 0.40.

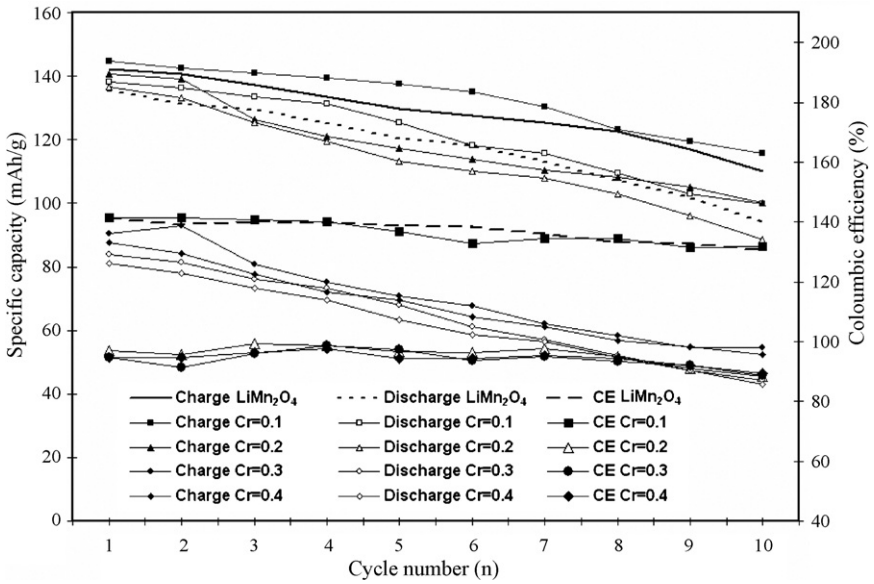


Fig. 11. Cycling performance of $LiMn_2O_4$ and $LiCr_xMn_{2-x}O_4$ with different Cr-doping levels, viz., 0.10, 0.20, 0.30 and 0.40.

capacity. It is apparent that high degree of Cr doping results in lowering of discharge capacity. While considering the cycling stability and columbic efficiency low doping of chromium is found to be beneficial. $LiCr_{0.1}Mn_{1.9}O_4$ electrodes deliver discharge capacity of 138 mAh $g^{-1}$ against the charge capacity of 144 mAh $g^{-1}$ yielding 95% columbic efficiency during the first cycle. These cells show a slow fading cycling behaviour. Over the 10 cycles these cells deliver 100 mAh $g^{-1}$ amounting to capacity fade of 3.8 mAh/(g cycle). The cells exhibit capacity fade of 4.8, 4.3 and 4.1 mAh/(g cycle) with Cr content of 0.20, 0.30 and 0.40, respectively. The high order of capacity fading observed with bare and Cr doped $LiMn_2O_4$ samples may also be due to the possible oxygen deficiency [31,32] arising from calcination at high temperature (850 °C). The capacity fade realized for low chromium spinel ($LiCr_{0.1}Mn_{1.90}O_4$) is low (3.8 mAh/(g cycle)) when compared to other doping concentrations and the un-doped one. Hence, $LiMn_2O_4$ spinel synthesized using phthalic acid with 0.1 Cr performs well in terms of low capacity fading characteristics over the 10 cycles.

### 3.6. Cyclic voltammetry

Cyclic voltammogram of $LiMn_2O_4$ recorded in the potential range 2.5–5.0 V at a scan rate of 1 mV $s^{-1}$ is presented in Fig. 12(a). A single anodic peak observed at 4.75 V is corresponding to $Mn^{3+}/Mn^{4+}$ couple and a cathodic peak

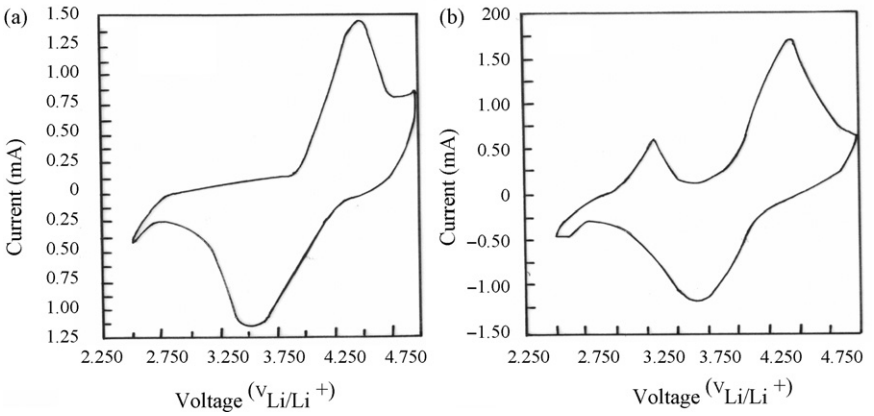


Fig. 12. Cyclic voltammograms of (a) $Li/LiMn_2O_4$; (b) $Li/LiCr_{0.1}Mn_{1.90}O_4$. Scan rate: 1 mV $s^{-1}$.

observed at 3.75 V is associated to $Mn^{4+}/Mn^{3+}$ couple [30]. Fig. 12(b) illustrates the cyclic voltammogram of $LiCr_{0.1}Mn_{1.90}O_4$ swept between 2.5 and 5.0 V at a scan rate of 1 mV $s^{-1}$. In this case, two anodic peaks are observed around 3.2 and 4.5 V corresponding to $Mn^{3+}/Mn^{4+}$ and $Cr^{3+}/Cr^{4+}$ couple. A single broad cathodic peak observed around 3.3 V is attributed to $Cr^{4+}/Cr^{3+}$ couple. As the scan rate of 1 mV $s^{-1}$ is fairly high, two separate peaks for $Mn^{4+}/Mn^{3+}$ and $Cr^{4+}/Cr^{3+}$ appeared as a single broad peak. $LiCr_{0.1}Mn_{1.90}O_4$ spinel exhibits slightly higher cathodic peak current (1.75 mA) when compared to the un-doped one (1.45 mA). This observation suggests that low level of chromium doping in the spinel enhances better electrochemical performance [33,34] of this compound.

## 4. Conclusions

A new chelating agent (phthalic acid) has been used for the first time in the sol–gel synthesize of $LiCr_xMn_{2-x}O_4$ ($x = 0.00$–$0.40$) spinel structured compound to use as a cathode material in lithium rechargeable batteries. XRD studies confirm the formation of single-phase product. SEM studies reveal that the particles with low chromium concentrations ($x = 0.10$ and 0.20) appear as individual grains of average grain size below 100 nm. TEM images of $LiCr_xMn_{2-x}O_4$ particles with high chromium (0.40) present as well-separated grain boundary with individual grain morphology. The discharge capacity and cycling performance of $LiCr_{0.1}Mn_{1.90}O_4$ spinel was found to deliver 138 mAh $g^{-1}$ as first cycle discharge capacity. Over the 10 cycles these cells deliver 100 mAh $g^{-1}$ amounting to capacity fade of 3.8 mAh/(g cycle), which is low when compared to other doping concentrations and the un-doped one.

## Acknowledgements

Dr. R. Thirunakaran is grateful to Royal Society, London, for awarding Post Doctoral Fellowship and thankful to Prof. Duncan Gregory, University of Glasgow for his able guidance. Thanks also due to Dr. Emina Hadzifejzovic and Dr. Jinhan Yao for their co-operative helps during his stay at Glasgow. Further, Dr. R. Thirunakaran is thankful to Prof. A.K. Shukla, Director, CECRI and CSIR for granting leave to avail the above fellowship.

## References

[1] J.M. Tarascon, W.R. McKinnon, F. Coowar, T.N. Bowner, G. Amatucci, D. Guyomard, J. Electrochem. Soc. 141 (1994) 1421.
[2] R.J. Gummow, A. de Kock, M.M. Thackeray, Solid State Ionics 69 (1994) 59.
[3] M.M. Thackeray, A. de Koch, M.H. Rossow, D. Liles, J. Electrochem. Soc. 139 (1992) 363.
[4] Y. Xia, M. Yoshio, J. Electrochem. Soc. 144 (1997) 2593.
[5] G. Pistoia, A. Antonini, R. Rosati, D. Zane, Electrochim. Acta 41 (1996) 2863.
[6] R.J. Gummow, A. Dckock, M.M. Thackeray, Solid State Ionics 69 (1994) 59.
[7] D.H. Jang, J.Y. Shin, S.M. Oh, J. Electrochem. Soc. 143 (1996) 2204.
[8] A. Amada, J. Solid State Chem. 122 (1996) 100.
[9] T. Ohuzuku, S. Takeda, M. Iwanaga, J. Power Sources 81/82 (1999) 90.
[10] M. Javed Iqbal, S. Zahoor, J. Power Sources 165 (2007) 393.
[11] M. Javed Iqbal, M.R. Siddiquah, J. Alloys Compd. 453 (2008) 513.
[12] J.H. Lee, J.K. Hong, D.H. Jang, Y.K. Sun, S.M. Oh, J. Power Sources 89 (2000) 7.
[13] S.H. Park, K.S. Park, Y.K. Sun, K.S. Nahm, J. Electrochem. Soc. 147 (2000) 2116.
[14] S. Bach, M. Henry, N. Baffier, J.J. Livage, Solid State Chem. 80 (1990) 325.
[15] J.P. Pereira-Romas, J. Power Sources 54 (1995) 120.
[16] P. Barboux, J.M. Tarascon, F.K. Shokoohi, J. Solid State Chem. 94 (1991) 185.
[17] W. Liu, G.C. Farrington, F. Chaput, B.J. Dunn, J. Elelectrochem. Soc. 143 (1993) 879.
[18] M.S. Whittingam, Solid State Ionics 86 (1996) 88.
[19] D. Shu, G. Kumar, K.-B. Kim, K.S. Ryu, S.H. Chang, Solid State Ionics 160 (2003) 227.
[20] X. Wang, X. Chen, L. Gao, H. Zhenug, M. Ji, T. Shen, Z. Zhang, J. Crystal Growth 256 (2003) 123.
[21] R. Thirunakaran, K.-T. Kim, Y.-M. Kang, C.-Y. Seo, J. Young-Lee, J. Power Sources 137 (2004) 199.
[22] R. Thirunakaran, K.-T. Kim, Y.-M. Kang, J. Young-Lee, Mater. Res. Bull. 40 (2005) 177.
[23] G.T.K. Fey, C.-Z. Lu, T. Premkumar, Mater. Chem. Phys. 80 (2003) 309.
[24] S.W. Jang, H.Y. Lee, K.C. Shin, S.M. Lee, J.K. Lee, S.J. Lee, H.K. Baik, D.S. Rhee, J. Power Sources 88 (2000) 274.
[25] R. Kalai Selvan, C.O. Augustin, C. Sanjeeviraja, V.G. Pol, A. Gedanken, Mater. Chem. Phys. 99 (2006) 109.
[26] J.-Y. Luo, X.-L. Li, Y.-Y. Xia, Electrochim. Acta 52 (2007) 4525.
[27] S.B. Park, S.M. Lee, H.C. Shin, W.I. Chob, H. Jang, J. Power Sources 166 (2007) 219.

[28] X. He, J. Li, Y. Cai, Y. Wang, J. Ying, C. Jiang, C. Wan, J. Power Sources 150 (2005) 216.
[29] J. Tu, X.B. Zhao, J. Xie, G.S. Cao, D.G. Zhuang, T.J. Zhu, J.P. Tu, J. Alloys Compd. 432 (2007) 313.
[30] D. Zhang, B.N. Popov, R.E. White, J. Power Sources 76 (1998) 81.
[31] J.M. Tarascon, D. Guyomard, Electrochim. Acta 38 (1993) 1221.
[32] Y. Xia, M. Yoshio, J. Electrochem. Soc. 143 (1996) 825.
[33] Sigala, D. Guyomard, A. Verbaere, Y. Piffard, M. Tournoux, Solid State Ionics 81 (1995) 167.
[34] H. Kuwai, M. Nagata, H. Tukamoto, A.R. West, J. Power Sources 81/82 (1999) 67.